

## Jet substructure measurements in pp and Pb–Pb collisions at $\sqrt{s_{\text{NN}}} = 5.02$ TeV with ALICE

James Mulligan for the ALICE Collaboration<sup>a,b</sup>

<sup>a</sup>Nuclear Science Division, Lawrence Berkeley National Laboratory, Berkeley, California 94720, USA

<sup>b</sup>Physics Department, University of California, Berkeley, CA 94720, USA

E-mail: [james.mulligan@berkeley.edu](mailto:james.mulligan@berkeley.edu)

We report jet substructure measurements in pp and Pb–Pb collisions at  $\sqrt{s_{\text{NN}}} = 5.02$  TeV with the ALICE detector. Charged-particle jets were reconstructed at midrapidity with the ALICE tracking detectors using the anti- $k_T$  algorithm with resolution parameters  $R = 0.2$  and  $R = 0.4$ . In pp collisions, the groomed jet momentum fraction,  $z_g$ , and the groomed jet radius,  $\theta_g \equiv R_g/R$ , are measured for the first time using the Dynamical Grooming method. Additionally, new systematic measurements of the infrared and collinear (IRC) safe ungroomed jet angularities are presented. In heavy-ion collisions, we measure  $z_g$  and  $\theta_g$  with the Soft Drop grooming algorithm. The large underlying event in heavy-ion collisions poses a challenge for the reconstruction of groomed jet observables, since fluctuations in the background can cause groomed splittings to be misidentified. By using strong grooming conditions to reduce this background, we report these observables fully corrected for detector effects and background fluctuations for the first time, and compare them to several theoretical models.

*HardProbes2020*

*1-6 June 2020*

*Austin, Texas*

## 1. Introduction

The substructure of jets can be used to study fundamental aspects of QCD in both pp and Pb–Pb collisions [1]. Jet grooming techniques, such as Soft Drop [2] and Dynamical grooming [3], reduce non-perturbative effects in pp collisions by selectively removing soft large-angle radiation, which allows for well-controlled comparisons of measurements to pQCD calculations [4–7]. Grooming techniques have also been applied to heavy-ion collisions, in order to explore whether jet quenching in the quark-gluon plasma modifies the hard substructure of jets [8–16]. Several measurements of groomed jet observables have been made in pp and heavy-ion collisions at the LHC and RHIC [17–22]. Ungroomed observables, such as jet angularities [23], provide a complementary way to study QCD in both pp and Pb–Pb [17, 24, 25] collisions, and offer the ability to systematically vary the observable definition in a way that is theoretically calculable, and give sensitivity to the predicted scaling of non-perturbative shape functions [26, 27].

In what follows, we reconstruct charged-particle jets at midrapidity with the ALICE [28] tracking detectors using the anti- $k_T$  algorithm [29, 30] with resolution parameters  $R = 0.2$  and  $R = 0.4$ . All presented results are corrected for detector effects (in both pp and Pb–Pb collisions) and background fluctuations (in Pb–Pb collisions) using an iterative unfolding algorithm [31].

## 2. Jet substructure in proton–proton collisions

### 2.1 Dynamical grooming in proton–proton collisions

The Dynamical grooming algorithm [3] identifies a single “splitting” by re-clustering the constituents of a jet with the Cambridge–Aachen algorithm [32], and traversing the primary Lund plane [33] to identify the splitting that maximizes:  $z_i(1-z_i)p_{T,i} \left(\frac{\Delta R_i}{R}\right)^a$ , where  $z_i$  is the longitudinal momentum fraction of the  $i^{\text{th}}$  splitting,  $\Delta R_i$  is the rapidity–azimuth ( $y, \varphi$ ) separation of the daughters, and  $a$  is a continuous free parameter. Since the grooming condition defines a maximum rather than an explicit cut (as in the case of Soft Drop), every jet will always return a tagged splitting. We focus on the two kinematic observables that characterize the splitting: the groomed jet radius,  $\theta_g \equiv R_g/R \equiv \sqrt{\Delta y^2 + \Delta \varphi^2}/R$ , and the groomed momentum fraction,  $z_g \equiv p_{T,\text{subleading}}/(p_{T,\text{leading}} + p_{T,\text{subleading}})$ .

Figure 1 shows the  $z_g$  and  $\theta_g$  distributions in pp collisions for several values of the grooming parameter  $a$ . For small values of  $a$ , the grooming condition favors splittings with symmetric longitudinal momentum, which is reflected in the distributions skewing towards large- $z_g$  and small- $\theta_g$ . As  $a$  increases, the grooming condition favors splittings with large angular separation, which is reflected in the distributions skewing towards small- $z_g$  and large- $\theta_g$ . The results are compared to PYTHIA [34], which describes the data well.

### 2.2 Ungroomed jet angularities in proton–proton collisions

The class of IRC-safe jet angularities [23] are defined as

$$\lambda_\beta^\kappa = \sum_{i \in \text{jet}} \left( \frac{p_{T,i}}{p_{T,\text{jet}}} \right)^\kappa \left( \frac{\Delta R_i}{R} \right)^\beta \quad (1)$$

for  $\kappa = 1$  and  $\beta > 0$ .

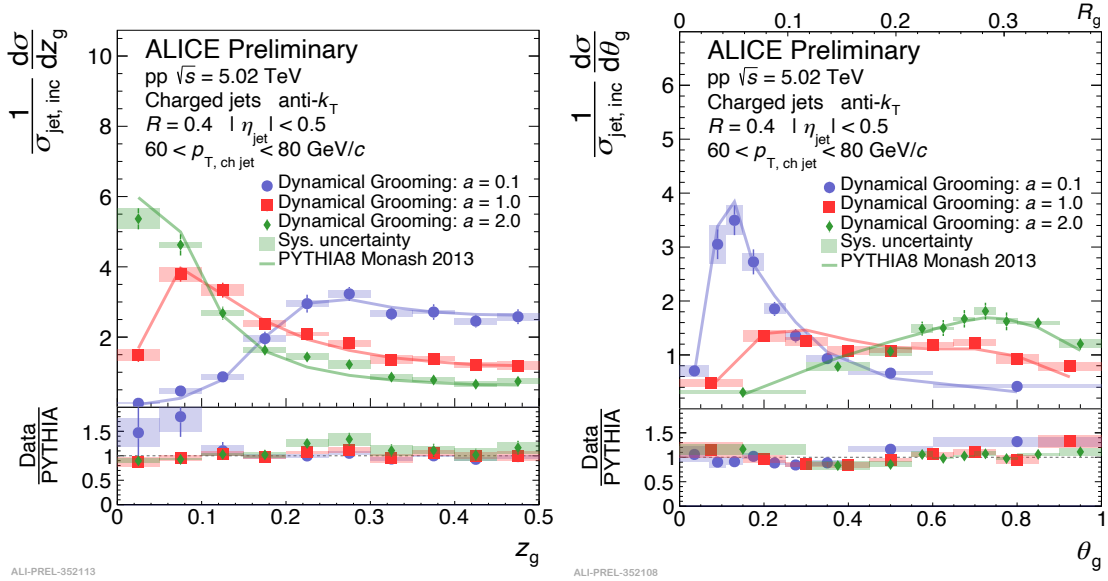


**Figure 1:** Measurements of  $z_g$  (left) and  $\theta_g$  (right) in pp collisions with Dynamical grooming [3] for three values of the grooming parameter  $a$ , along with comparison to PYTHIA Monash 2013 [34].

Figure 2 shows the  $\lambda_\beta^{\kappa=1}$  distributions in pp collisions for  $R = 0.2$  (left) and  $R = 0.4$  (right) for several values of  $\beta$ . As  $\beta$  increases, the distributions skew towards small  $\lambda_\beta^{\kappa=1}$ , since  $\Delta R_i/R$  is smaller than unity. For larger  $R$ , the distributions are narrower than for smaller  $R$ , as expected due to the collinear nature of jet fragmentation. The results are compared to PYTHIA [34], which describes the data reasonably well but with some deviations to be further explored.

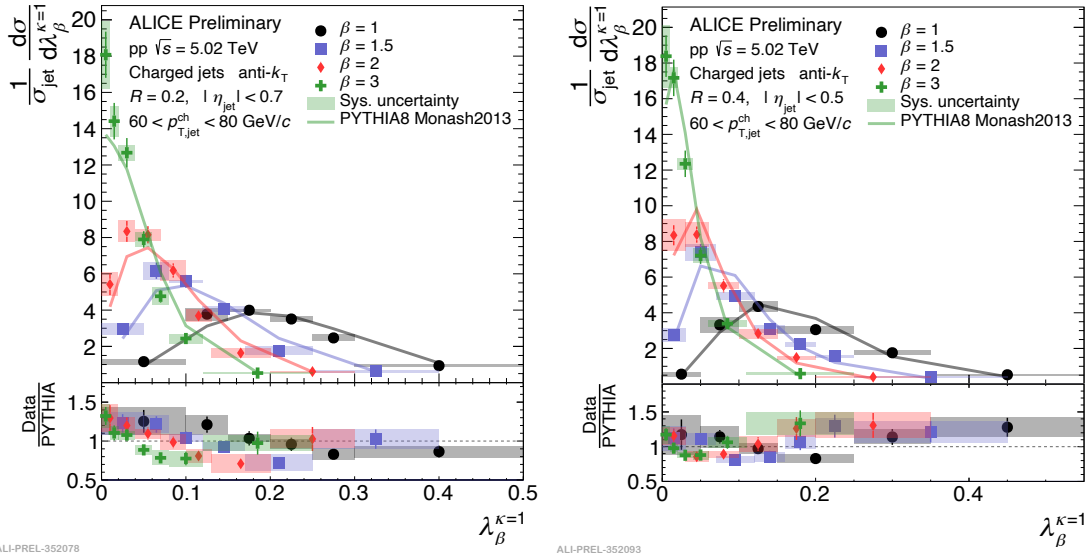


**Figure 2:** Measurements of jet angularities  $\lambda_\beta^{\kappa=1}$  in pp collisions with for  $R = 0.2$  (left) and  $R = 0.4$  (right) for four values of the continuous parameter  $\beta$ , along with comparison to PYTHIA Monash 2013 [34].

### 3. Jet substructure in heavy-ion collisions

In heavy-ion collisions, the large underlying event poses a challenge for the reconstruction of groomed jet observables, since fluctuations in the background can cause groomed splittings to be misidentified [35]. We present measurements [36] of  $z_g$  and  $\theta_g$  with the Soft Drop grooming algorithm that are fully corrected for detector effects and background fluctuations, leveraging stronger grooming conditions than in previous measurements. Figures 3 and 4 show these measurements in Pb–Pb collisions together with their comparison to those from pp collisions, for central (0–10%) and semi-central (30–50%) Pb–Pb collisions, respectively.

We find that the  $z_g$  distributions in Pb–Pb collisions are consistent with those in pp collisions, whereas a significant narrowing of the  $\theta_g$  distributions in Pb–Pb collisions relative to pp collisions is observed. These measurements are compared to a variety of jet quenching models: JETSCAPE [37–39], Caucal et al. [13, 40], Chien et al. [8], Qin et al. [10], Pablos et al. [15, 41, 42], and Yuan et al. [14, 43]. All models considered are consistent with the  $z_g$  measurements. Many of the models capture the narrowing effect observed in the  $\theta_g$  distributions, although with quantitative differences. This behavior is consistent with models implementing an incoherent interaction of the jet shower constituents with the medium, but also consistent with medium-modified “quark/gluon” fractions with fully coherent energy loss. By isolating the theoretically well-controlled hard substructure of jets, these measurements provide direct connection to specific jet quenching physics mechanisms, and offer the opportunity for future measurements to definitively disentangle them.

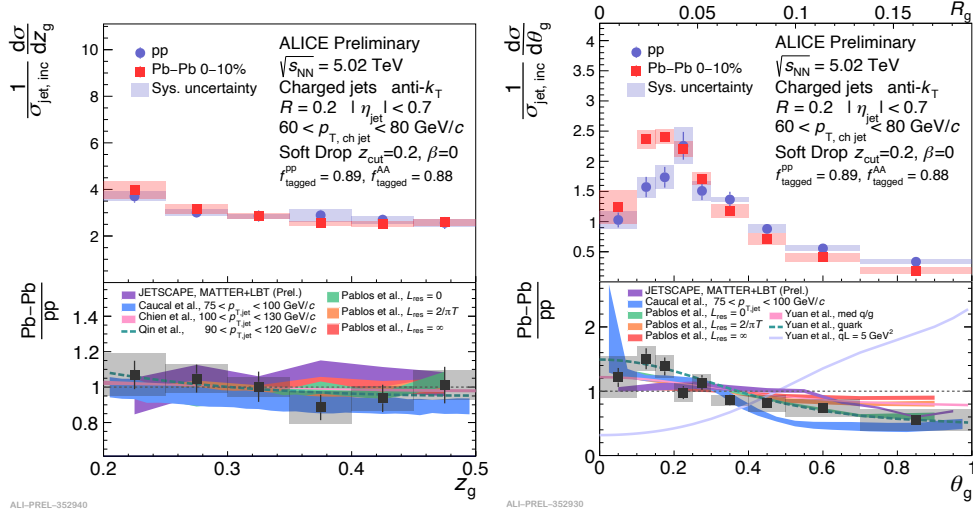


**Figure 3:** Measurements of  $z_g$  (left) and  $\theta_g$  (right) in 0–10% central Pb–Pb collisions compared to pp collisions for  $R = 0.2$ , along with comparison to several theoretical models [36].

### References

- [1] A. J. Larkoski, I. Moult and B. Nachman, *Physics Reports* **841** (2020), 1–63.
- [2] A. J. Larkoski, S. Marzani, G. Soyez and J. Thaler, *JHEP* **05** (2014), 146.
- [3] Y. Mehtar-Tani, A. Soto-Ontoso and K. Tywoniuk, *PRD* **101** (2020), 034004.
- [4] M. Dasgupta, A. Fregoso, S. Marzani and G. P. Salam, *JHEP* **09** (2013), 029.
- [5] A. J. Larkoski, S. Marzani and J. Thaler, *PRD*. **91** (2015), 111501.
- [6] Y. Mehtar-Tani, A. Soto-Ontoso and K. Tywoniuk, [arXiv:2005.07584](https://arxiv.org/abs/2005.07584).

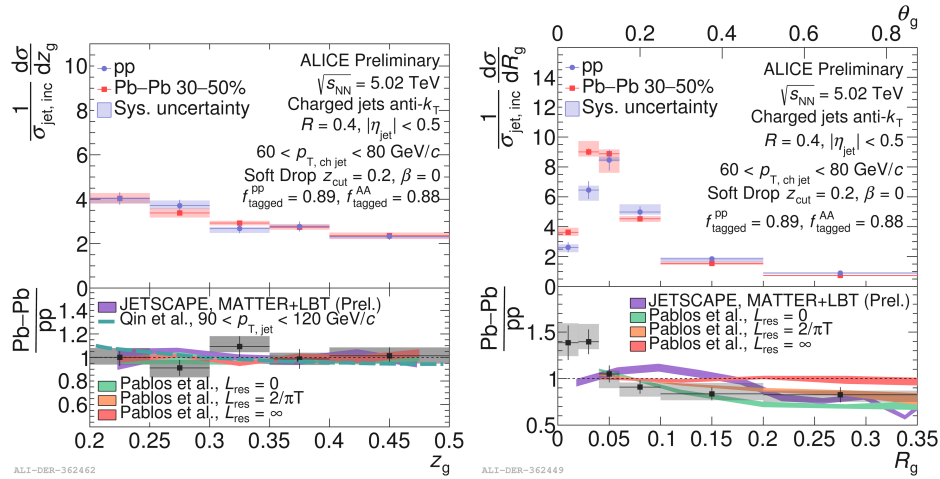


**Figure 4:** Measurements of  $z_g$  (left) and  $R_g$  (right) in 30–50% central Pb–Pb collisions compared to pp collisions for  $R = 0.4$ , along with comparison to several theoretical models [36].

- [7] Z.-B. Kang, K. Lee, X. Liu, D. Neill and F. Ringer, *JHEP* **2020** (2020), 54.  
 [8] Y.-T. Chien and I. Vitev, *PRL* **119** (2017), 112301.  
 [9] Y. Mehtar-Tani and K. Tywoniuk, *JHEP* **2017** (2017), 125.  
 [10] N.-B. Chang, S. Cao and G.-Y. Qin, *PLB* **781** (2018), 423–432.  
 [11] G. Milhano, U. A. Wiedemann and K. C. Zapp, *PLB* **779** (2018), 409.  
 [12] R. Kunnawalkam Elayavalli and K. C. Zapp, *JHEP* **7** (2017), 141.  
 [13] P. Caucal, E. Iancu and G. Soyez, *JHEP* **10** (2019), 273.  
 [14] F. Ringer, B.-W. Xiao and F. Yuan, *PLB* **808** (2020), 135634.  
 [15] J. Casalderrey-Solana, G. Milhano, D. Pablos and K. Rajagopal, *JHEP* **01** (2020), 044.  
 [16] H. A. Andrews and et al., *JPG* **47** (2020), 065102.  
 [17] CMS Collaboration, *PRD* **98** (2018), 092014.  
 [18] ATLAS Collaboration, *PRD* **101** (2020), 052007.  
 [19] STAR Collaboration, *arXiv:2003.02114*.  
 [20] CMS Collaboration, *PRL* **120** (2018), 142302.  
 [21] ALICE Collaboration, *PLB* **802** (2020), 135227.  
 [22] CMS Collaboration, *JHEP* **2018** (2018), 161.  
 [23] A. J. Larkoski, J. Thaler and W. J. Waalewijn, *JHEP* **2014** (2014), 129.  
 [24] ATLAS Collaboration, *PRD* **86** (2012), 072006.  
 [25] ALICE Collaboration, *JHEP* **2018** (2018), 139.  
 [26] Z.-B. Kang, K. Lee and F. Ringer, *JHEP* **2018** (2018), 110.  
 [27] Z.-B. Kang, K. Lee, X. Liu and F. Ringer, *PLB* **793** (2019), 41.  
 [28] ALICE Collaboration, *J. Instrum.* **3** (2008), S08002.  
 [29] M. Cacciari, G. P. Salam and G. Soyez, *JHEP* **04** (2008), 063.  
 [30] M. Cacciari, G. P. Salam and G. Soyez, *EPJC* **72** (2012), 1896.  
 [31] G. D’Agostini, *NIM A* **362** (1995), 487.  
 [32] Y. Dokshitzer, G. Leder, S. Moretti and B. Webber, *JHEP* **1997** (1997), 001.  
 [33] F. A. Dreyer, G. P. Salam and G. Soyez, *JHEP* **2018** (2018), 64.  
 [34] T. Sjostrand and et al., *CPC* **191** (2015), 159.  
 [35] J. Mulligan and M. Ploskon, *arXiv:2006.01812*.  
 [36] ALICE Collaboration, ALICE-PUBLIC-2020-006, <https://cds.cern.ch/record/2725572>.  
 [37] JETSCAPE Collaboration, *arXiv:1903.07706*.  
 [38] Y. He, T. Luo, X.-N. Wang and Y. Zhu, *PRC* **91** (2015), 054908.  
 [39] A. Majumder, *PRC* **88** (2013), 014909.  
 [40] P. Caucal, E. Iancu, A. Mueller and G. Soyez, *PRL* **120** (2018), 232001.  
 [41] J. Casalderrey-Solana, D. C. Gulhan, J. G. Milhano, D. Pablos and K. Rajagopal, *JHEP* **019** (2014), 019.  
 [42] Z. Hulcher, D. Pablos and K. Rajagopal, *JHEP* **010** (2018), 10.  
 [43] J.-W. Qiu, F. Ringer, N. Sato and P. Zurita, *PRL* **122** (2019), 252301.